International Journal of
Automotive Manufacturing and Materials（IJAMM）

Scilight

Article

Investigating Spray Characteristics of Synthetic Fuels: Comparative Analysis with Gasoline

Weidi Huang [1,2], Mitsuharu Oguma [2], Koichi Kinoshita [2,*], Yohko Abe [2], and Kotaro Tanaka [1,3]

[1] Carbon Recycling Energy Research Centre, Ibaraki University, 4-12-1 Nakanarusawa, Hitachi 316-8511, Japan
[2] Research Institute for Energy Conservation, National Institute of Advanced Industrial Science and Technology, Namiki 1-2-1, Tsukuba 305-8564, Japan
[3] Graduate School of Science and Engineering, Ibaraki University, 4-12-1 Nakanarusawa, Hitachi 316-8511, Japan
* Correspondence: koichi-kinoshita@aist.go.jp
Received: 13 March 2024; Revised: 22 May 2024; Accepted: 31 May 2024; Published: 5 June 2024

Abstract: Studying synthetic fuels is imperative due to their potential to offer sustainable alternatives to conventional fossil fuels, thereby addressing environmental concerns, enhancing energy security, and facilitating the transition to cleaner and more efficient transportation systems. This study presents an experiment analysis concentrating on spray characteristics of five types of synthetic fuels (bio-naphtha, EtG, G40, bio-ethanol, and DMC) in a comparison with gasoline. The experiment was conducted ranging from non-evaporated conditions to evaporated conditions, to thoroughly assess the spray behavior of the tested fuels. Results showed that EtG and G40 share similar properties with conventional gasoline. The discharge coefficient (*Cd*) was found to increase closely linearly with the square root of fuel density. Under non-evaporated condition (T_a = 25 °C), except for DMC, the spray tip penetration of other fuels deviates within ±5% compared to gasoline. Under evaporated condition (T_a = 200 °C), EtG maintains a spray tip penetration within ±5% of gasoline, while bio-naphtha, G40, and DMC fall within ±10% of gasoline. Notably, bio-ethanol shows a 12% higher penetration compared to gasoline, likely due to its slower evaporation and higher latent heat of vaporization.

Keywords: synthetic fuels; fuel properties; spray characteristics; evaporated conditions; schlieren imaging

1. Introduction

Synthetic fuels are artificially produced fuels using carbon dioxide (CO_2) and hydrogen (H_2) as raw materials. Comparable to conventional petroleum products, synthetic fuels encompass a spectrum of hydrocarbons, enabling bespoke fabrication tailored to distinct applications such as gasoline or kerosene. Notably, synthetic fuels derived from “green hydrogen”, synthesized through renewable energy sources, are denoted as “e-fuels” [1]. While the electrification of passenger vehicles is gaining traction within the automotive industry, electric vehicles (EVs) encounter hurdles including limited range, extended charging times, restricted payload capacity, and infrastructural constraints. These challenges are further compounded in the realm of commercial vehicles like trucks, rendering the transition to electrification a multifaceted approach [2].

Consequently, the adoption of alternative fuels, such as e-fuels, is anticipated alongside conventional options to address these challenges in commercial vehicle electrification. Multiple reports employing well-to-wheel analyses and life cycle assessments have underscored the comparable CO_2 emission reduction potential of internal combustion engines (ICEs) fueled by e-fuels as EVs. This is due to the negative well-to-tank CO_2 emissions associated with e-fuels [3–5]. Given the massive ICEs still existing, it is important to explore e-fuels as a viable alternative fueling solution to expedite the decarbonization process.

In March 2023, the European Union (EU) made a landmark decision by endorsing the continued utilization of internal combustion engine (ICE) vehicles fueled by e-fuels beyond 2035, marking a significant milestone in sustainable transportation policies [6]. This decision signifies the growing global recognition of e-fuels as a practical alternative in the transition towards cleaner mobility systems. Subsequently, in May 2023, the Ministry of Economy, Trade, and Industry (METI) announced a strategic policy revision aimed at accelerating the timeline for the commercial deployment of e-fuels to the early 2030s, a notable advancement from the previous target of 2040 [7]. This shift was spurred by Europe's progressive policy adjustment permitting the usage of internal combustion engines powered by e-fuels.

E-fuels, as synthetic derivatives, exhibit diverse molecular structures [8]. Their unique physical properties and chemical compositions of e-fuels are crucial consideration for future engine specifications, necessitating a delicate balance between cost considerations and synthetic methodologies. Predominantly, extant research has concentrated on elucidating the intricacies of e-fuel manufacturing processes [9,10], assessing their operational efficiency [11,12], and conducting comprehensive life cycle analyses [7]. These endeavors aim to furnish a holistic understanding of e-fuels, thereby facilitating informed decision-making processes across various sectors.

The utilization of e-fuels in engine applications has been relatively underexplored in current research literature. However, there have been many studies on synthetic fuels. Pastor et al. [13] shared an investigation of oxymethylene dimethyl ethers (OME) when blended with diesel in an optical engine setup. Their findings unveiled enhanced in-cylinder soot reduction, particularly evident under low oxygen conditions, with varying piston geometries. Similarly, Novella et al. [14] conducted a numerical exploration of OME, optimizing combustion systems to achieve heightened efficiency (approximately 2.2%) and a noteworthy 35.7% reduction in NO_x emissions compared to baseline engines. Betgeri et al. [15] meanwhile, probed into neat 1-Octanol and its blends with diesel, observing heightened ignition sensitivity alongside substantial reductions in smoke and carbon monoxide emissions. Notably, the existing literature predominantly revolves around diesel-like fuels, with scant attention given to gasoline-like alternatives.

In 2021, the Japanese New Energy and Industrial Technology Development Organization (NEDO) embarked on a groundbreaking project with a primary emphasis on advancing the Fischer-Tropsch (FT) reaction of e-fuels, with the aim of spearheading the evolution of FT processes [16]. As part of the NEDO initiative, an extensive survey was conducted to evaluate numerous synthetic fuels available worldwide. The survey unearthed notable disparities in physical and chemical properties between synthetic fuels and traditional fossil fuels, with engine testing currently in the scheduling phase.

This study proposes an experimental investigation focusing on the spray characteristics of five types of synthetic fuels, juxtaposed with gasoline. The experimental initial conditions range from non-evaporated to evaporated conditions, aiming to provide a comprehensive examination of the spray characteristics exhibited by the tested fuels. Moreover, this study also delves into the relationship between spray characteristics and fuel properties. In the short term, this investigation seeks to enhance the utilization efficiency of existing synthetic fuels in engines. In the long term, a combination of chemical simulation and computational fluid dynamics (CFD) simulation will be employed to ultimately propose the most optimized design and utilization of e-fuels for future e-fueled engines.

2. Description of Experiments

2.1. Tested Fuels

This study has examined the spray characteristics of five different types of synthetic fuels, namely EtG (ethanol-to-gasoline), G40 (comprising 10% bio-ethanol, 30% MtG (Methanol to gasoline), and 60% gasoline by volume), bio-naphtha, DMC (dimethyl carbonate), and bio-ethanol, alongside conventional gasoline (as outlined in Table 1). EtG, G40, and bio-naphtha are blended compositions, while DMC and bioethanol are singular substances. Specifically, DMC, bio-ethanol, and G40 samples were sourced from the Karlsruhe Institute of Technology (KIT). Bioethanol, derived from biomass sources, and DMC, synthesized from CO_2 and bio-methanol, represent sustainable alternatives. G40 formulation adheres to the EN228 standards [17]. EtG and bio-naphtha were obtained from Coryton Advanced Fuels Ltd. [18]. EtG, synthesized from bio-

ethanol, mirrors the functional attributes of fossil-derived gasoline meeting EN228 standards. Bio-naphtha, on the other hand, originates from biomass via the FT process.

Table 1. Tested fuels and their sources.

Fuels	Sources
Bio-Naphtha	by Coryton Advanced Fuels Ltd.
Gasoline	JIS #2 by domestic gas station
G40	by the Karlsruhe Institute of Technology
EtG	By Coryton Advanced Fuels Ltd.
Bio-ethanol	by the Karlsruhe Institute of Technology
DMC	by the Karlsruhe Institute of Technology

In terms of fuel property comparisons, domestic gasoline sourced from a Japanese gas station was included as a reference purposes. It's noteworthy to note that despite being produced synthetically, DMC and Bioethanol analyzed in this study are pure substances. Their fuel properties, spray characteristics, and combustion behavior are expected to align with previous investigations [19,20]. Nevertheless, the spray characteristics of DMC and ethanol have been included for comparative analysis alongside the other fuels examined in this study.

The fuel density of the tested fuels was directly assessed utilizing the Anton Paar DMA 4100M Tester, renowned for its precision measurements within a range of 0 to 3 g/cm³ with an accuracy of 0.0001 g/cm³. Notably, the fuel density measurements were conducted at a standardized temperature of 15 °C. The temperature control mechanism of the tester boasts a remarkable accuracy of 0.03 °C. The comprehensive technical specifications can be referred to reference [21].

Moreover, the viscosity of the tested fuels was gauged employing the Yoshida-Kagagu VB-X6 Tester, adhering to measurement standards stipulated by JIS K2283, ASTM 445, 446, and IP71. The instrumentation details can be found in reference [22].

The chemical properties of the synthetic fuels were examined utilizing an HP 6890 Series Gas Chromatograph (GC), with data processing facilitated through HP ChemStation (Agilent Technologies). Within the GC setup, the liquid fuel samples underwent vaporization to transform them into gas form. Subsequently, the gaseous samples, facilitated by a carrier gas such as helium or nitrogen, traversed through the GC column. The specific GC column employed in this study was the HP-DHA1, featuring a diameter of 0.25 mm and a film thickness of 0.5 μm. This specialized column served the purpose of segregating and analyzing the individual components of the vaporized fuel. As the components exited the column, they were detected via a Flame Ionization Detector (FID), which measured the concentration of each component and generated chromatographic data. Each component present in the sample gas elicited a distinctive peak in the chromatogram, with the controller discerning the identity of each component based on its retention time—the interval from the initiation of the analysis cycle to the apex of the peak. By juxtaposing the chromatogram against established standards, the components within the liquid fuel samples could be identified, along with their respective quantities. The methodological insights can be found in reference [23].

2.2. Testing Nozzle

For the investigation, a commercial Gasoline Direct Injection (GDI) injector was employed. This injector model features six holes, designed in a hole-and-counterbore configuration. Such a configuration is commonly utilized in GDI engines to facilitate enhanced spray breakup [24,25]. A schematic depiction of the internal structure of the test nozzle is presented in Figure 1, accompanied by a summary of its geometric parameters in Table 2. Notably, all holes within the injector possess identical diameters for both the hole and

counterbore. However, the length of each hole varies depending on its inclining angle.

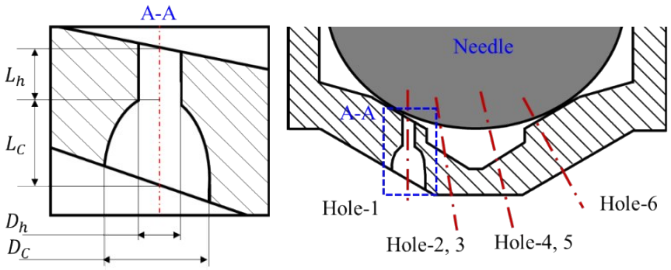

Figure 1. Nozzle internal structure and geometric parameters.

Table 2. Geometric parameters of the testing nozzle.

Nozzle	Hole Diameter (D_h/mm)	Hole Length (L_h/mm)	Counterbore Diameter (D_c/mm)	Counterbore Length (L_c/mm)
Hole-1	0.13	0.30	0.36	0.30

2.3. Experimental Methods

Figure 2 illustrates schematically the schlieren imaging setup implemented in this study. The comprehensive test rig comprises a common rail injection system, a control unit, a constant volume vessel, and an LED-based imaging system. Utilizing the same high-speed camera (Model SA-Z, Photron Inc.), schlieren images capturing shock waves were acquired. The specifications for image acquisition were configured with a frame rate of 75,000 Hz, an image resolution of 512 × 496 pixels, and a pixel size of 0.147 mm. More details about the test rig setup can be found in reference [26].

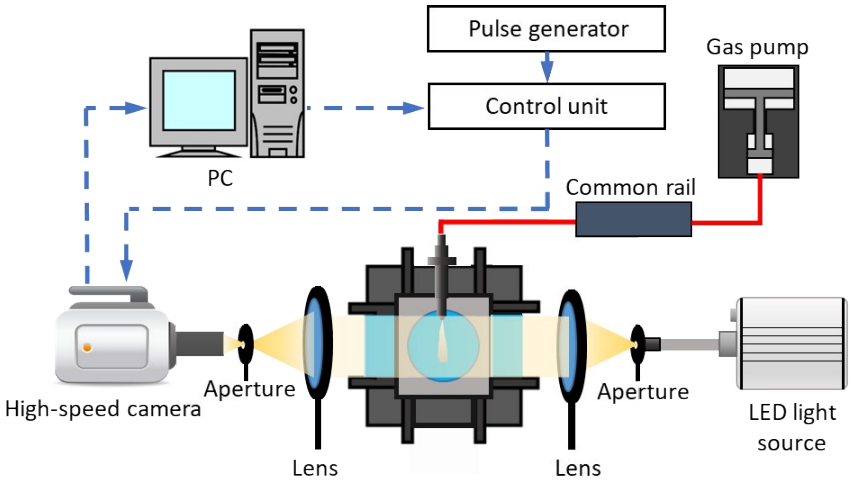

Figure 2. Experimental setup for schlieren imaging.

The spray chamber is equipped with eight embedded heating rods within its metallic structure, enabling the ambient gas temperature inside the chamber to reach up to 200 °C. Through a gradual heating process, it was observed that the temperature of the chamber body (in close proximity to the nozzle tip) and the ambient gas temperature equilibrated. This phenomenon can be attributed to the specialized design of the spray chamber, featuring a minimal inner volume (approximately 500 mL). To ensure temperature uniformity during measurements, a low measuring frequency (0.2 Hz) was adopted. Consequently, the fuel temperature within the nozzle and the ambient gas temperature were considered identical for the purposes of this study.

Ambient gas temperatures spanning 25 °C and 200 °C were selected for investigation, encompassing the spectrum from non-evaporated to evaporated states of the spray characteristics. To optimize fuel breakup and

evaporation, the ambient gas density (ρ_a) was maintained at a fixed value of 2 kg/m³. Injection pressures (P_{in}) of 25 MPa were employed, with a constant injection duration (t_{inj}) set at 2 ms. Each testing condition was subjected to ten repetitions to ensure robustness and reliability of the experimental data. The initial experimental parameters are succinctly summarized in Table 3.

Table 3. Initial experiment conditions.

Initial Conditions	
Injection pressure	25 MPa (±1 MPa)
Injection pulse width	2.0 ms
Ambient gas temperature	25 °C (non-evaporated), 200 °C (evaporated)
Ambient gas density	CO_2 under 2 kg/m^3
Measuring repetitions	Ten shots

2.4. Data Analysis

A custom imaging processing program was developed using MATLAB to analyze the original schlieren images captured by the high-speed camera. As illustrated in Figure 3, a typical image undergoes processing stages before and after image manipulation. Initially, the original spray image is divided by the background image (depicted in Figure 3b) to eliminate fixed noise from the background. This step facilitates the acquisition of a spray image with a uniform background. Leveraging Figure 3b, a false-coloring image of the spray can be generated (as depicted in Figure 3d), which emphasizes the grayscale differences at each pixel. In schlieren measurements, these grayscale differences correspond to variations in fuel density, serving as indicators of differences in evaporation status.

Utilizing the adaptive grayscale thresholding algorithm provided by MATLAB [27], the image is subsequently binarized (as shown in Figure 3e) based on Figure 3b. The binarized image enables the extraction of two crucial parameters: spray tip penetration and spray area. The former reflects the penetration capability of the spray, whereas the latter indicates the overall extent and outline of the spray.

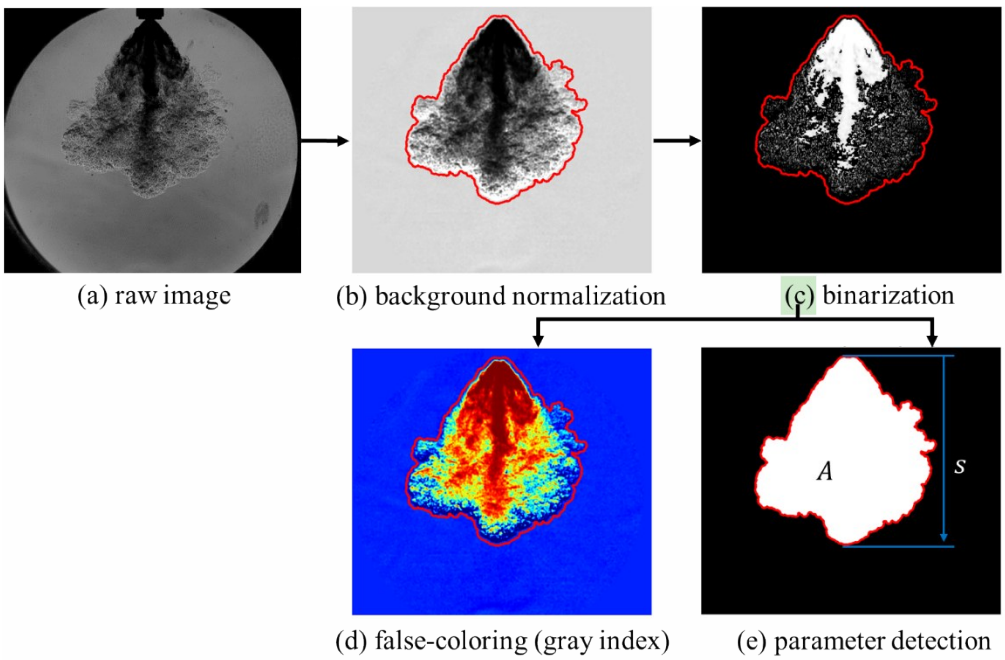

Figure 3. Image processing and data analysis.

3. Experimental Results

3.1. Fuel Properties

Figure 4 illustrates the physical and chemical properties of the tested fuels, with corresponding values detailed in Table 4. Notably, EtG and G40, engineered to emulate conventional gasoline, exhibit similar properties to gasoline itself. G40, owing to its bio-ethanol fraction, boasts a higher Research Octane Number (RON) of 105.0 compared to gasoline (92.2) and EtG (91.2). Conversely, bio-naphtha, characterized by a high fraction of light paraffins, manifests a lower RON of 55.9, alongside diminished Higher Heating Value (HHV) and lower fuel density relative to gasoline.

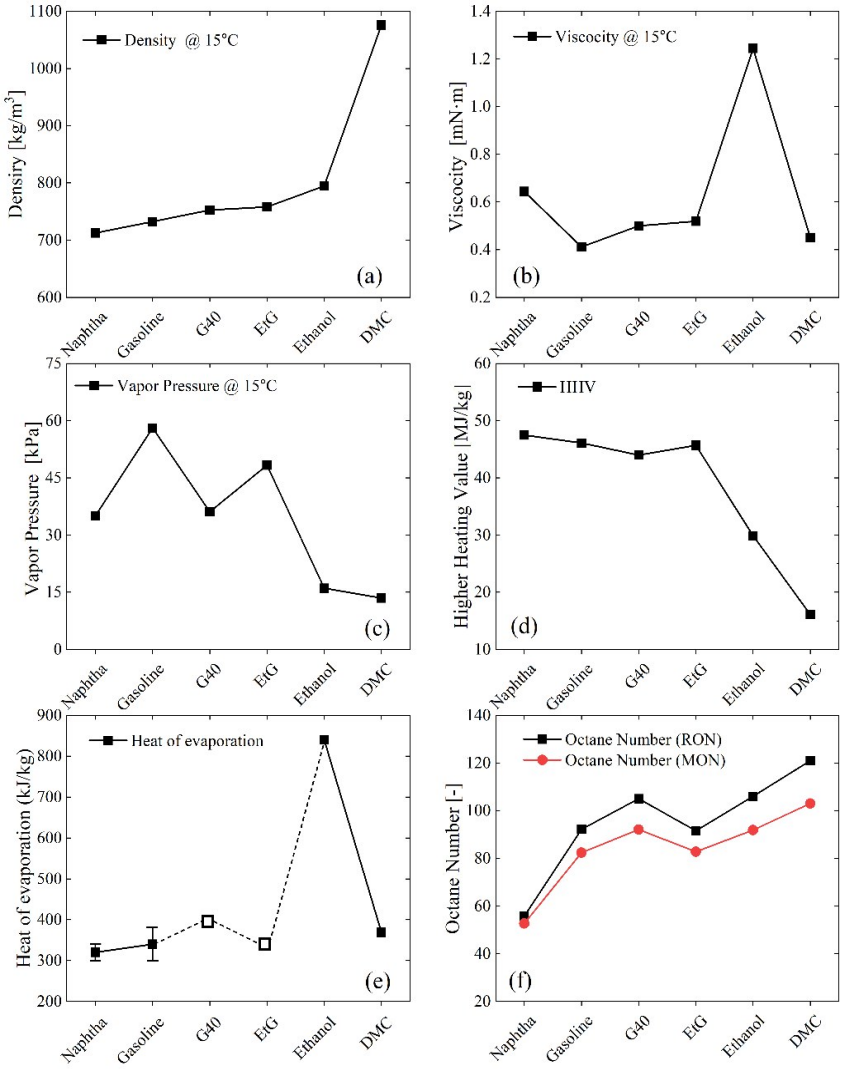

Figure 4. Key physical and chemical properties of the tested fuels: (**a**) densities; (**b**) viscosities; (**c**) vapor pressures; (**d**) Higher Heating Value (HHD); (**e**) heat of evaporation; (**f**) Research Octane Number (RON) and MON values.

Furthermore, the properties of bio-ethanol and DMC closely align with those observed in previous investigations [19,20], regardless of their specific manufacturing routes. DMC and bio-ethanol exhibit lower vapor pressures compared to other fuels. Given the evaporated conditions under study, considerations of latent heat of vaporization are significant. However, the absence of measuring capability for latent heat necessitated recourse to literature surveys. According to available literature, gasoline and naphtha exhibit latent heats ranging from 300–380 kJ/kg [28,29], while DMC's fixes at 369 kJ/kg [28]. Ethanol's latent heat (840 kJ/kg [20]) significantly distinguishes it from these fuels. Consequently, it is believed that G40's latent heat is greater than that of gasoline and EtG due to its ethanol content.

Table 4. Properties of testing fuels (at 15 °C and ambient pressure).

Fuels	ρ_f [kg/m^3]	μ [mPa·s]	P_s [kPa]	ΔH_{vap} [kJ/kg]	HHV [MJ/kg]	RON -
Bio-Naphtha	712.6	0.6441	34.7	300–340	47.5	55.9
Gasoline	732.3	0.4111	58.1	300–380	46.1	92.2
G40	752.7	0.4999	36.1	-	44.0	105.0
EtG	752.8	0.5192	48.6	-	45.9	91.3
Ethanol	794.5	1.2442	16.1	840	29.9	106.0
DMC	1076.4	0.4510	13.5	369	16.1	51.5

3.2. Mass Flow Rate

The discharge coefficient (*Cd*) of an injector is a critical parameter that characterizes the flow rate performance of the injector. It represents the ratio of the actual mass flow (M_{exp}) to the theoretical mass flow (M_{th}), as described by Equation (1).

$$Cd = M_{exp}/M_{th} \tag{1}$$

M_{th} can be computed utilizing Equation (2), adhering to Bernoulli's law.

$$M_{th} = n \times A \times \sqrt{2\Delta P \times \rho_f} \tag{2}$$

where the Δp denotes the pressure differential between the nozzle sac and the ambient gas, while ρ_f represents the fuel density. Parameters n and A correspond to the number of nozzle orifices and the cross-sectional area of the orifice, respectively. M_{exp} was quantified using a commercial tester (Ono FJ-7000), with detailed specifications provided in reference [30]. In the mass flow rate measurement experiments, each test condition was repeated five times to ensure accuracy and consistency. Our analysis indicated that the deviation in the mass flow rate measurements was less than 1%. Consequently, the averaged mass flow rate data was utilized for the calculation of the discharge coefficient (Cd), incorporating the fuel density.

Figure 5a illustrates a nearly linear correlation between *Cd* and the square root of density. Notably, bio-naphtha, characterized by the lowest density, exhibited the lowest *Cd*, whereas DMC, possessing the highest density, demonstrated the highest *Cd*. This observed trend aligns with prior research, underscoring that higher fuel density can enhance flow discharging area by mitigating flow separation within the nozzle orifice [31].

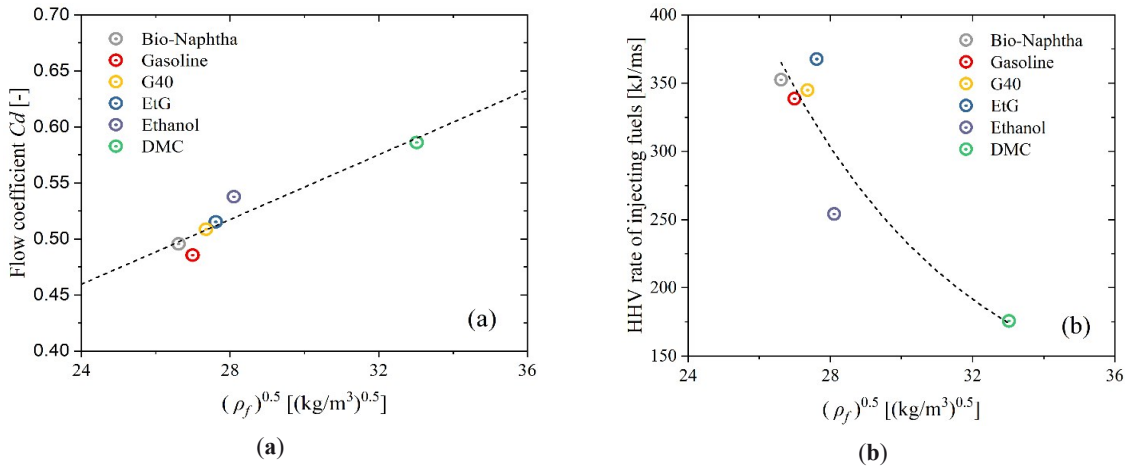

(a) **(b)**

Figure 5. Flow coefficient of tested fuels: (**a**) flow discharge coefficient of injection; (**b**) HHV rate of injection.

Furthermore, Figure 5b showcases the net calorific values of ethanol and DMC, approximating half and one-third of gasoline, respectively. Consequently, injecting the same fuel energy into the combustion chamber necessitates a prolonged injection duration. Extended injection durations may compromise combustion efficiency in engines due to inferior control over the combustion process. The experimental findings thus suggest that the actual injection duration of bio-ethanol and DMC, particularly when utilized in blends, may be reduced owing to their higher *Cd*. This revelation bears significant implications for the integration of these fuels into internal combustion engines.

3.3. Spray Characteristics under Non-Evaporated Condition

Figure 6 presents the spray characteristics of various fuels under a non-evaporated condition, with five distinct spray plumes discernible in the images. It's important to note that, owing to the nozzle arrangement, the spray plume in the middle actually comprises two overlapping spray plumes. From the observations, it's evident that under non-evaporative conditions, the spray plumes exhibit clear separation from each other. In terms of spray morphology and development, particularly regarding penetration capability, it is observed that the spray development of EtG and bio-ethanol appears slightly stronger compared to other fuels.

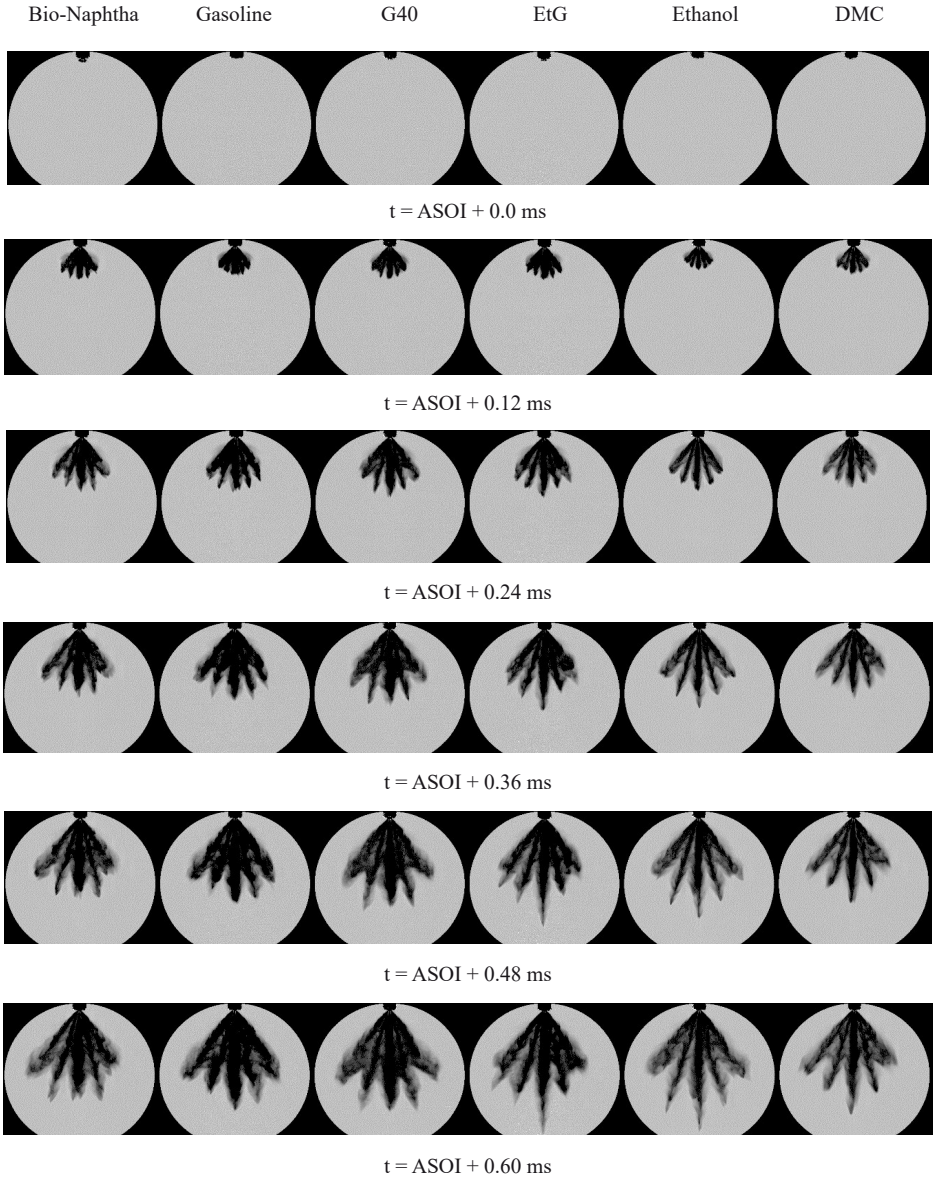

Figure 6. Spray characteristics of varied fuels under non-evaporated condition (T_a = 25 °C).

Figure 7 illustrates the spray tip penetration of different fuels under the non-evaporative condition. In Figure 7a, the variation of spray tip penetration over time is depicted, while Figure 7b presents the relative spray tip penetration of each fuel compared to gasoline at a fixed time of 0.8 ms. From the figures, it is evident that the spray tip penetration of DMC is notably shorter compared to other fuels, approximately 91% of gasoline's penetration at the fixed time of 0.8 ms. In contrast, the spray tip penetration of other fuels remains within the range of ±5% compared to gasoline.

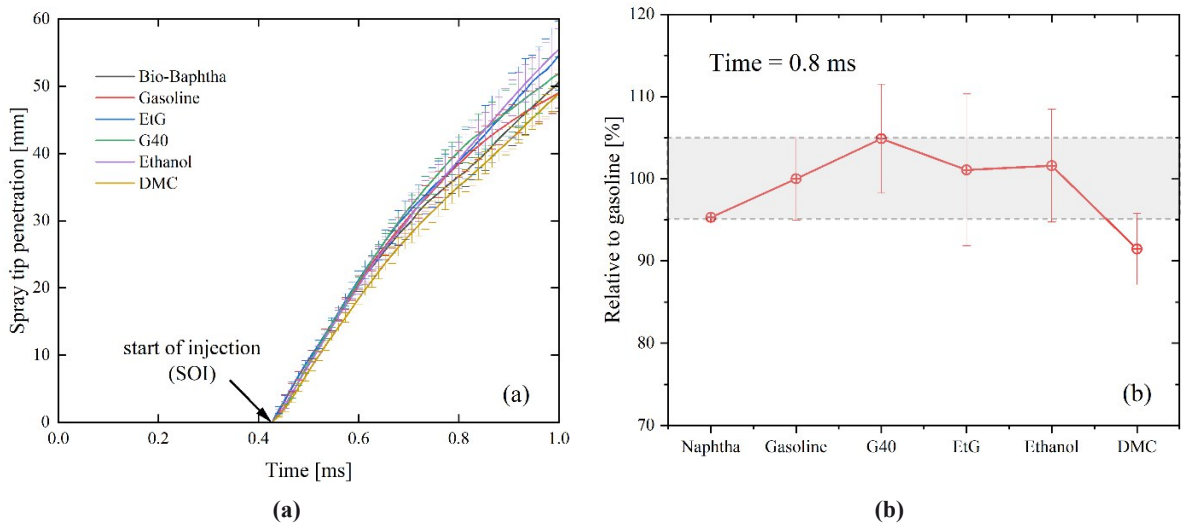

Figure 7. Spray tip penetration of varied fuels under non-evaporated condition (T_a = 25 °C): (**a**) spray tip penetration over time; (**b**) the relative one compared to gasoline at a fixed time of 0.8 ms.

3.4. Spray Characteristics under Evaporated Condition

Figure 8 illustrates the spray characteristics of various fuels under an evaporated condition. In this condition, characterized by high fuel temperature and low ambient pressure, the occurrence of flash boiling spray is anticipated. This phenomenon is particularly pronounced for bio-ethanol and DMC, with boiling temperatures of approximately 78 °C and 89 °C, respectively. In the presented images, rapid vaporization is evident, and the spacing between plumes disappears completely, consistent with the characteristics of flash boiling. Notably, the penetration capability of bio-ethanol and G40 appears longer compared to other fuels. Furthermore, the brightness variations in the schlieren images also reflect changes in fuel density. Darker areas in the spray images indicate higher density and lower fuel evaporation. It is observed that the overall brightness of the ethanol fuel spray is lower compared to other fuels, indicating a lower degree of fuel evaporation.

In this experiment, the schlieren measurement technique was utilized for photography. This technique is adept at detecting changes in the refractive index, which are caused by variations in air density. Such changes are particularly useful for visualizing the evaporative characteristics of the spray. Consequently, it is able to observe the shock fronts at t = ASOI + 0.12 ms in Figure 8. These shock fronts are believed to be compression waves in the air that occur concurrently with the initiation of fuel injection.

Figure 9 displays the spray tip penetration of various fuels under the evaporative condition. Figure 9a illustrates the variation of spray tip penetration over time, while Figure 9b compares the relative penetration to gasoline at a fixed time of 0.8 ms. It is evident from the figures that the spray tip penetration of bio-ethanol and G40 exceeds that of other fuels. Specifically, at a fixed time of 0.8 ms, EtG maintains a spray tip penetration within ±5% of gasoline. Meanwhile, bio-naphtha, G40, and DMC fall within ±10% of gasoline. However, bio-ethanol surpasses this range, exhibiting a 12% higher penetration compared to gasoline.

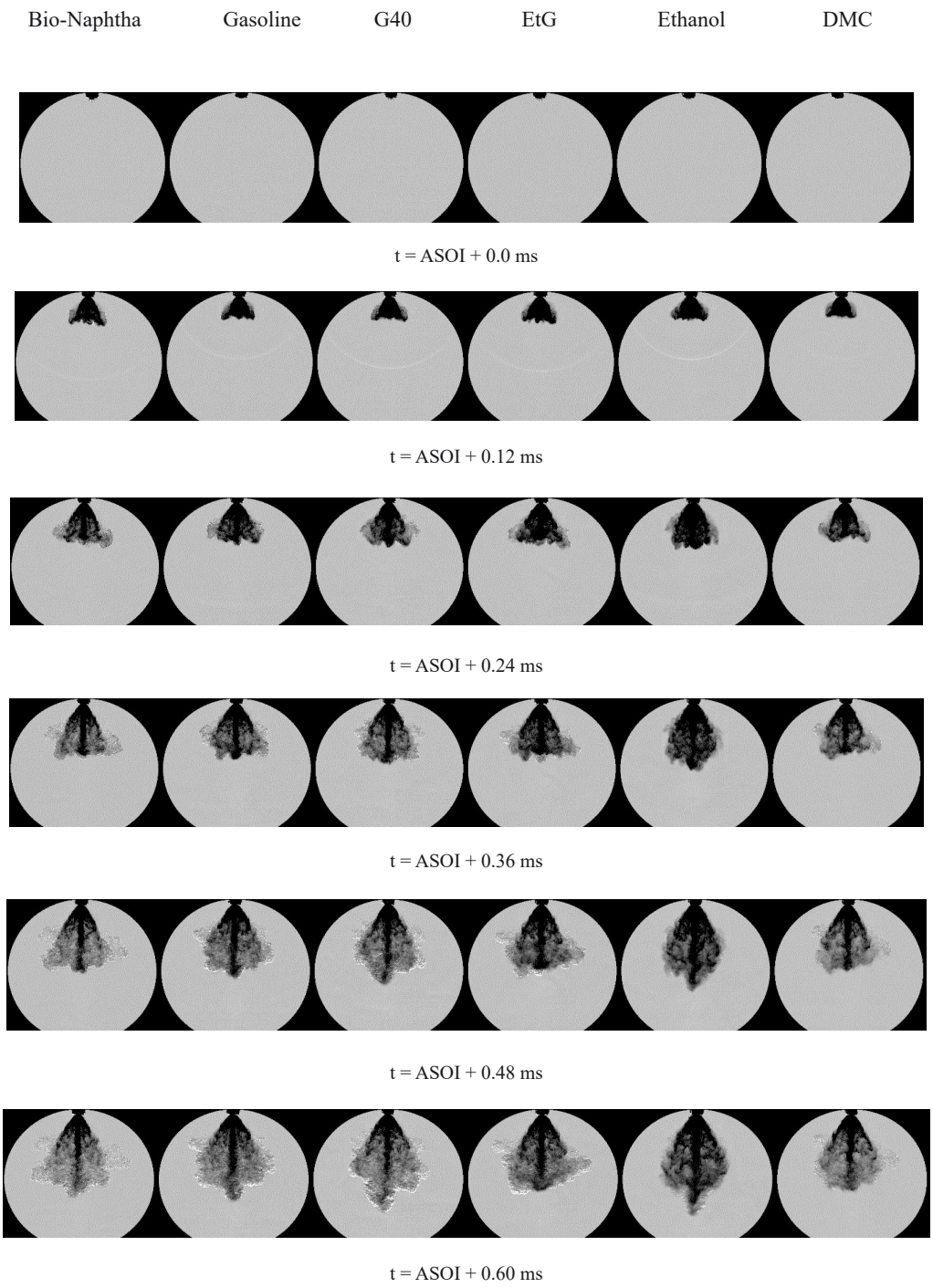

Figure 8. Spray characteristics of varied fuels under evaporated condition (T_a = 200 °C).

It might be noted that bio-naphtha and DMC always have the shortest penetration under both non-evaporated and evaporated conditions. The classical penetration formula by Hiroyasu and Arai [32] suggests that penetration is inversely related to fuel density, which could explain DMC's consistently short penetration due to its higher density. For bio-naphtha, initial spray tip penetration is comparable to that of gasoline, EtG, and G40. However, the penetration capacity declines after a distance of approximately t = ASOI + 0.6 ms. This decrease may be linked to the air-fuel interaction; with lower fuel density, air entrainment intensifies, causing greater radial spray expansion at the expense of axial penetration [33]. Thus, the relatively low penetration for bio-naphtha and DMC is likely due to a combination of factors that merit further investigation.

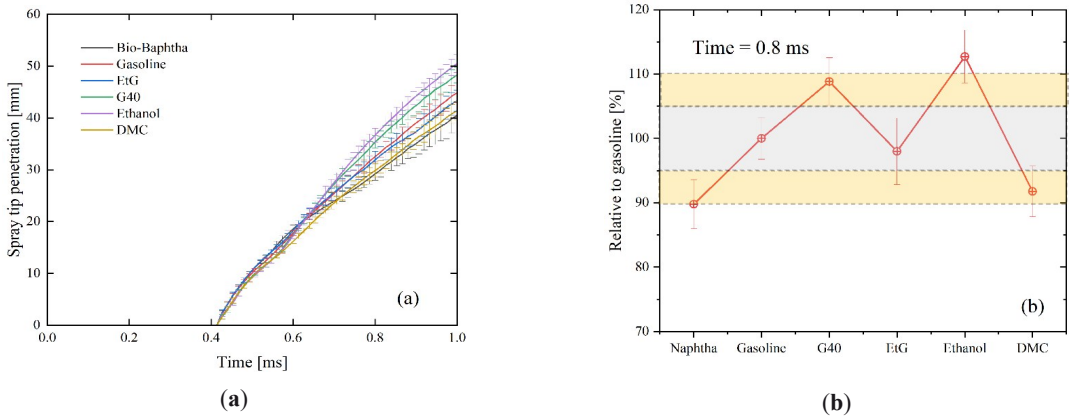

(a) **(b)**

Figure 9. Spray tip penetration of varied fuels under non-evaporated condition (T_a = 200 °C): (**a**) spray tip penetration over time; (**b**) the relative one compared to gasoline at a fixed time of 0.8 ms.

Figure 10 illustrates the spray area under evaporative conditions. Figure 10a presents the spray area without gray-level indexing, while Figure 10b depicts the weighted spray area with gray-level indexing. The former delineates the overall extent and outline of the spray, whereas the latter reflects the evaporation status of the spray. The weighted spray area computation incorporates the grayscale value of each pixel. This approach emphasizes darker pixels, typically indicative of denser regions within the spray, thereby providing a more refined evaluation of the spray's spatial distribution and density, particularly relevant for understanding the evaporation process and variations in fuel characteristics.

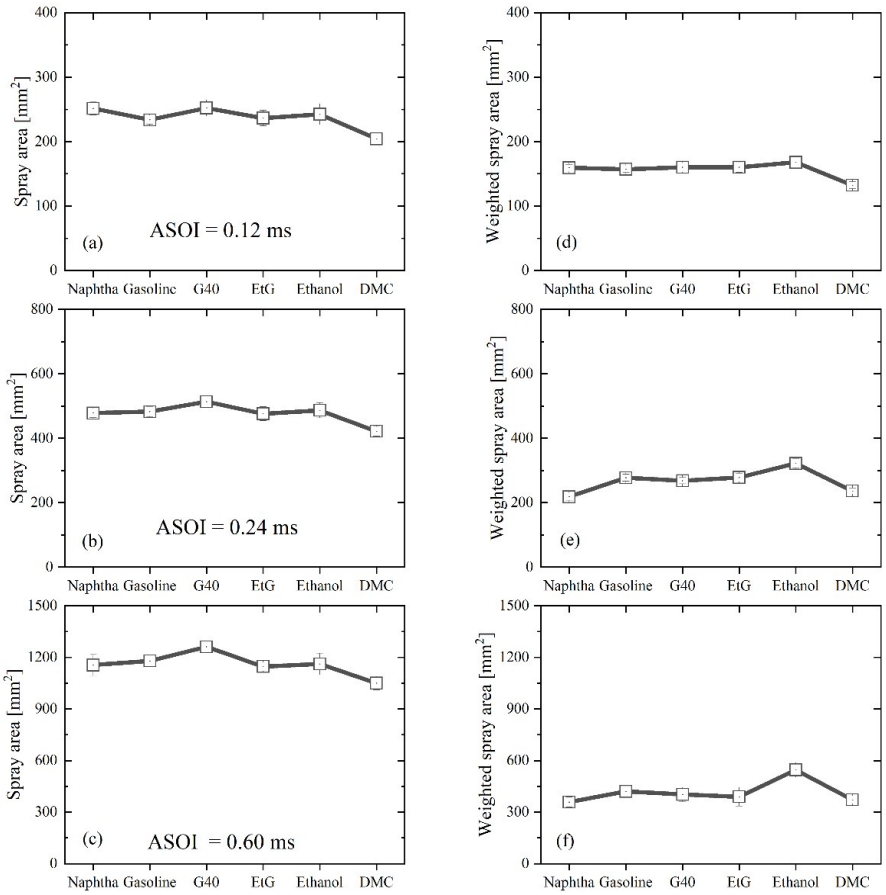

Figure 10. Spray area under evaporating conditions (Ta = 200 °C): (**a** – **c**) spray area without the grayscale indexed; (**d**–**f**) weighted spray area with grayscale indexed.

Observing the figures, it is apparent that during the initial stages of fuel injection (Figure 10a, d), the spray area and weighted spray area exhibit proximity, indicating incomplete commencement of spray evaporation. As time progresses, both parameters increase, but the rate of increase in spray area surpasses that of the weighted spray area, signifying ongoing spray evaporation. Comparing different fuels, it is evident that the weighted spray area of bio-ethanol consistently outstrips that of other fuels at all time points, indicative of slower bio-ethanol evaporation. This phenomenon likely stems from bio-ethanol's higher latent heat of vaporization. In contrast, for other fuels, both the spray area and weighted spray area exhibit relatively similar trends across various time points, consistent with the assumption of comparable latent heats of vaporization among these fuels.

4. Conclusions

This study proposes an experiment concentrating on spray characteristics of five types of synthetic fuels (bio-naphtha, EtG, G40, bio-ethanol, and DMC) in a comparison with gasoline. The experimental initial conditions range from non-evaporated conditions to evaporated conditions, which aimed to provide a detailed examination of spray characteristics of the tested fuels. Discussions have also been made to interpret the relationship of the spray characteristics with fuel properties. The key findings of this study can be summarized below.

(1) EtG and G40 share similar properties with conventional gasoline, while G40 showing a higher Research Octane Number (RON) compared to gasoline and EtG, likely attributed to its bio-ethanol content. Bio-naphtha exhibits a lower RON, reduced Higher Heating Value (HHV), and lower fuel density compared to gasoline. The properties of bio-ethanol and DMC align closely with previous investigations, irrespective of their production methods.

(2) The discharge coefficient (*Cd*) exhibits a close linear relationship with the square root of density. Specifically, bio-naphtha, with the lowest density, displays the lowest *Cd*, while DMC, the densest, has the highest *Cd*. This implies that the actual injection duration of bio-ethanol and DMC, particularly in blends, may be reduced due to their higher *Cd*.

(3) Under non-evaporated condition (T_a = 25 °C), DMC shows a slightly shorter spray tip penetration compared to other fuels, approximately 91% of gasoline's penetration at a fixed time of 0.8 ms. The spray tip penetration of other fuels remains within the range of ±5% compared to gasoline.

(4) Under evaporated condition (T_a = 200 °C), EtG maintains a spray tip penetration within ±5% of gasoline at a fixed time of 0.8 ms, while bio-naphtha, G40, and DMC fall within ±10% of gasoline. However, bio-ethanol shows a 12% higher penetration compared to gasoline. Its slower evaporation is indicated by a consistently larger weighted spray area, likely attributed to ethanol's higher latent heat of vaporization.

Author Contributions: Conceptualization, W.H.; methodology, W.H.; software, W.H., K.K. and Y.A.; validation, W.H., K.K. and Y.A.; formal analysis, W.H. and Y.A.; investigation, W.H., K.K. and Y.A.; resources, M.O.; data curation, W.H. and Y.A.; writing — original draft preparation, W.H.; writing — review and editing, K.K., M.O. and K.T.; visualization, W.H.; supervision, M.O. and K.T.; project administration, M.O. and K.T.; funding acquisition, M.O. All authors have read and agreed to the published version of the manuscript.

Funding: This research was funded by Research on Carbon Recycling and Next-Generation Thermal Power Generation Technologies, CO_2 Emission Reduction and Utilization Technologies, CO_2 Utilization Technologies for Liquid Fuels, and Next-Generation FT Reaction and Integrated Process for Liquid Synthetic Fuel Production of New Energy and Industrial Technology Development Organization (NEDO).

Institutional Review Board Statement: Not applicable.

Informed Consent Statement: Not applicable.

Data Availability Statement: Not applicable.

Acknowledgments: This research is one of the projects promoted by NEDO, managed by JPEC as a leader of the fuel utilizing working group of the NEDO project. The authors appreciate the financial support from NEDO, and the research collaboration with JPEC.

Conflicts of Interest: The authors declare no conflict of interest.

References

1. Ueckerdt, F.; Bauer, C.; Dirnaichner, A.; Everall, J.; Sacchi, R.; Luderer, G. Potential and risks of hydrogen-based e-fuels in climate change mitigation. *Nat. Clim. Chang.* **2021**, *11*, 384–393. https://doi.org/10.1038/s41558-021-01032-7.
2. Yu, X.; Sandhu, N.S.; Yang, Z.; Zheng, M. Suitability of energy sources for automotive application—A review. *Appl. Energy* **2020**, *271*, 115169. https://doi.org/10.1016/j.apenergy.2020.115169.
3. Alamia, A.; Magnusson, I.; Johnsson, F.; Thunman, H. Well-to-wheel analysis of bio-methane via gasification, in heavy duty engines within the transport sector of the European Union. *Appl. Energy* **2016**, *170*, 445–454. https://doi.org/10.1016/J.APENERGY.2016.02.001.
4. Prussi, M.; Laveneziana, L.; Testa, L.; Chiaramonti, D. Comparing e-Fuels and Electrification for Decarbonization of Heavy-Duty Transports. *Energies* **2022**, *15*, 8075. https://doi.org/10.3390/en15218075.
5. Garcia, A.; Monsalve-Serrano, J.; Villalta, D.; Tripathi, S. Electric Vehicles vs E-fuelled ICE Vehicles: Comparison of potentials for life cycle CO2 reductionemission. World Congress ExperienceWCX SAE, NumberPaper 2022-01-0745. *SAE Technical Paper* **2022**, 1–15. https://doi.org/10.4271/2022-01-0745.Received.
6. Exclusive: EU Drafts Plan to Allow E-Fuel Combustion Engine Cars|Reuters n.d. Available online: https://www.reuters.com/business/autos-transportation/eu-proposes-exception-e-fuel-combustion-engines-2035-2023-03-21/ (accessed on 24 May 2023).
7. R&D Related to Carbon Neutral Fuels—Japan Petroleum Energy Center (JPEC) n.d. Available online: https://www.pecj.or.jp/en/rd-related-to-carbon-neutral-fuels/ (accessed on 11 March 2024).
8. Ram, V.; Salkuti, S.R. An Overview of Major Synthetic Fuels. *Energies* **2023**, *16*, 2834. https://doi.org/10.3390/en16062834.
9. d'Amore, F.; Nava, A.; Colbertaldo, P.; Visconti, C.G.; Romano, M.C. Turning CO_2 from fuel combustion into e-Fuel? Consider alternative pathways. *Energy Convers. Manage.* **2023**;*289*. https://doi.org/10.1016/j.enconman.2023.117170.
10. Goh, B.H.H.; Chong, C.T.; Ong, H.C.; Seljak, T.; Katrašnik, T.; Józsa, V.; Ng, J.-H.; Tian, B.; Karmarkar, S.; Ashokkumar, V. Recent advancements in catalytic conversion pathways for synthetic jet fuel produced from bioresources. *Energy Convers. Manage.* **2022**, *251*, 114974. https://doi.org/10.1016/j.enconman.2021.114974.
11. Ballal, V.; Cavalett, O.; Cherubini, F.; Watanabe, M.D.B. Climate change impacts of e-fuels for aviation in Europe under present-day conditions and future policy scenarios. *Fuel* **2023**, *338*, 127316. https://doi.org/10.1016/j.fuel.2022.127316.
12. Hombach, L.E.; Doré, L.; Heidgen, K.; Maas, H.; Wallington, T.J.; Walther, G. Economic and environmental assessment of current (2015) and future (2030) use of E-fuels in light-duty vehicles in Germany. *J. Cleaner Prod.* **2019**, *207*, 153–162. https://doi.org/10.1016/j.jclepro.2018.09.261.
13. Pastor, J.V.; Micó, C.; Lewiski, F.; Tejada, F.J.; Tornatore, C. A Synergic Application of High-Oxygenated E-Fuels and New Bowl Designs for Low Soot Emissions: An Optical Analysis. *Appl. Sci.* **2023**, *13*, 8560. https://doi.org/10.3390/app13148560.
14. Novella, R.; Bracho, G.; Gomez-Soriano, J.; Fernandes, C.S.; Lucchini, T. Combustion system optimization for the integration of e-fuels (Oxymethylene Ether) in compression ignition engines. *Fuel* **2021**, *305*, 121580. https://doi.org/10.1016/j.fuel.2021.121580.
15. Betgeri, V.; Bhardwaj, O.P.; Pischinger, S. Investigation of the drop-in capabilities of a renewable 1-Octanol based E-fuel for heavy-duty engine applications. *Energy* **2023**, *282*, 128811. https://doi.org/10.1016/j.energy.2023.128811.
16. Development of Technology for Practical Use of CO_2 Emission Reduction and Effective Utilization n.d. Available online: https://www.nedo.go.jp/news/press/AA5_101410.html (accessed on 12 March 2024).
17. Refuel 2021—International Workshop on the Application of Carbon Neutral Fuel n d. Available online: https://www.ifkm.kit.edu/downloads/ReFuel2021_Proceedings_Global.pdf#page=12.58 (accessed on 31 May 2024).
18. Glossary—What are the different types of sustainable fuels?|Coryton n.d. Available online: https://coryton.com/lab/articles/glossary-what-are-the-different-types-of-sustainable-fuels/ (accessed on 13 March 2024).
19. Thakur, A.K.; Kaviti, A.K.; Mehra, R.; Mer, K.K.S. Progress in performance analysis of ethanol-gasoline blends on SI engine. *Renew. Sustainable Energy Rev.* **2017**, *69*, 324–340. https://doi.org/10.1016/j.rser.2016.11.056.
20. Properties of Ethanol at NIST n.d. Available online: https://webbook.nist.gov/cgi/cbook.cgi?ID=C64175&Mask=4 (accessed on 13 March 2024).
21. Manuel of Anton Paar DMA 4100M n. d. Available online: https://www. anton-paar. com/jp-jp/products/details/benchtop-density-meter-dma-4100-m/ (accessed on 12 March 2024).
22. Specifications of Yoshida-Kagagu VB-X*6* n.d. Available online: https://www.yoshida-kagaku.co.jp/pdf/nendo/1.pdf (accessed on 31 May 2024).
23. Gas Chromatography Fundamentals n.d. Available online: https://www.agilent.com/en/product/gas-chromatography/what-is-gas-chromatography (accessed on 22 August 2023).
24. Huang, W.; Moon, S.; Wang, J.; Murayama, K.; Arima, T.; Sasaki, Y.; Arioka, A. Nozzle tip wetting in gasoline direct injection injector and its link with nozzle internal flow. *Int. J. Engine Res.* **2019**, *21*, 340–351. https://doi.org/10.1177/1468087419869774.
25. Hélie, J.; Lamarque, N.; Fremaux, J.L.; Serrecchia, P.; Khosravi, M.; Berkemeier, O. The process of tip wetting at the spray injection end. *Int. J. Engine Res.* **2021**, *22*, 125–39. https://doi.org/10.1177/1468087419840842.
26. Huang, W.; Gong, H.; Moon, S.; Wang, J.; Murayama, K.; Taniguchi, H.; Arima, T.; Arioka ,A.; Sasaki, Y. Nozzle Tip Wetting in GDI Injector at Flash-boiling Conditions. *Int. J. Heat Mass Transfer* **2021**, *169*, 120935. https://doi.org/10.1016/j.ijheatmasstransfer.2021.120935.

27. MATLAB Imbinarize n.d. Available online: https://www.mathworks.com/help/images/ref/imbinarize.html (accessed on 13 March 2024).
28. Abdalla, A.O.G.; Liu, D. Dimethyl carbonate as a promising oxygenated fuel for combustion: A review. *Energies* **2018**, *11*, 1552. https://doi.org/10.3390/en11061552.
29. Specifications of Petroleum Naphtha n. d. Available online: https://cameochemicals. noaa. gov/chris/PTN. pdf (accessed on 13 March 2024).
30. Manual of Ono FJ-7000 n.d. Available online: https://www.onosokki.co.jp/HP-WK/products/keisoku/vehicle/fj7000.html (accessed on 12 March 2024).
31. Huang, W.; Pratama, R.H.; Oguma, M.; Kinoshita, K.; Takeda, Y.; Suzuki, S. Spray dynamics of synthetic dimethyl carbonate and its blends with gasoline. *Fuel* **2023**, *341*, 127696. https://doi.org/10.1016/j.fuel.2023.127696.
32. Hiroyasu, H.; Arai, M. Structures of fuel sprays in diesel engines. *SAE Technical Papers* **1990**, *99*, 1050–1061. https://doi.org/10.4271/900475.
33. Qureshi, M.M.R.; Zhu, C. Gas entrainment in an evaporating spray jet. *Int. J. Heat Mass Transfer* **2006**, *49*, 3417–3428. https://doi.org/10.1016/j.ijheatmasstransfer.2006.03.006.